ELSEVIER

Journal of Organometallic Chemistry 486 (1995) 37–43

Journal of Organometallic Chemistry

Synthesis and X-ray crystal structure of the heterometallic platinum–mercury cluster $[\{Pt_4(\mu\text{-}CO)_4(PMe_2Ph)_4\}\{\mu_3\text{-}HgI\}_2]$

Klaus-Hermann Dahmen [a,*], Daniel Imhof [a], Luigi M. Venanzi [a], Tobias Gerfin [b], Volker Gramlich [b]

[a] *Laboratorium für anorganische Chemie, ETH Zürich, Universitätsstrasse 6, CH-8092 Zürich, Switzerland*
[b] *Institut für Kristallographie und Petrographie, ETH Zürich, Sonneggstrasse 5, CH-8092 Zürich, Switzerland*

Received 27 February 1994

Abstract

The bicapped cluster $[\{Pt_4(\mu\text{-}CO)_4(PMe_2Ph)_4\}\{\mu_3\text{-}HgI\}_2]$ (1) was obtained by reacting the cluster compound $[Pt_4(\mu\text{-}CO)_5(PMe_2Ph)_4]$ with one equivalent of $[Hg_2I_2]$. The IR and multinuclear NMR data as well as the X-ray crystal structure of the compound are reported. This compound crystallizes in the monoclinic space group $P2_1/m$ with $Z = 4$, $a = 10.086(2)$, $b = 18.739(4)$, $c = 24.764(5)$ Å, and $\beta = 90.94(3)°$. The structure was refined to $R = 0.0787$ for 3303 observed reflections ($I \geq 3.0\sigma(I)$).

Keywords: Platinum; Mercury; Cluster; NMR-spectroscopy; X-ray structure; Heterobimetallics

1. Introduction

Trimetallic compounds such as $[Pt_3(\mu\text{-}CO)_3(PR_3)_3]$, (333); $[Pt_3(\mu\text{-}CO)_3(PR_3)_4]$, (334); $Pt_3(\mu\text{-}CNXyl)_2(\mu\text{-}CO)(CNXyl)(PCy_3)_2]$, $[Pt_3(\mu\text{-}CNXyl)_3(CNXyl)_2(PCy_3)]$, $[Pt_3(\mu\text{-}SO_2)_{3-x}(\mu\text{-}L)_x(PCy_3)_3]$, L = CNXyl, Cl, SO_2, CO, and $[Pt_3(\mu_3\text{-}CO)(dppm)_3]^{2+}$, dppm = $Ph_2PCH_2PPh_2$ can be used as building blocks for a wide variety of heterometallic clusters [1–17]. These are in general, addition products of one or more building blocks and a coordinatively unsaturated metal species. The structures of these heteronuclear clusters are of sandwich, I, half-sandwich, II or bicapped, III types. Selected examples are given in Table 1.

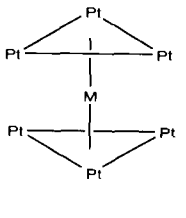

Type I

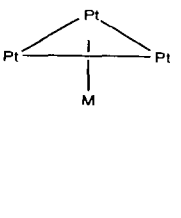

Type II

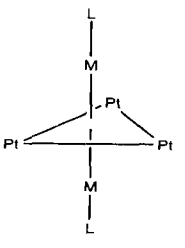

Type III

The observation that a large variety of main group or transition metals bind to mercury or mercury-containing fragments has stimulated the systematic synthesis of mixed metal clusters containing this element. Many such compounds have been described in a recent review by Gade [18].

Although platinum–mercury cluster compounds were reported (Table 1) only a few of them are obtained as addition products of platinum clusters with mercury compound.

A recent report described the formation of a new heterometallic cluster of type III by reacting $[Pt_3(\mu\text{-}CO)_3(PR_3)_3]$ with Hg_2X_2 [17]. In this reaction the mercury–mercury bond of the Hg_2X_2 is broken and each HgX fragment is attached on opposite sides of the Pt_3-unit, type III. Although these compounds have the bicapped structure in solution, they are dimeric in the solid state, shown in Scheme 1.

However, the clusters 4:5:4 of the type $[Pt_4(\mu\text{-}CO)_5(PR_3)_4]$ can also be used as building blocks for the synthesis of heterometallic clusters without a rearrangement of the basic Pt-skeleton. Starting from the structure of the 4:5:4 cluster one can imagine that the carbonyl ligand bridging the two central Pt-atoms can be easily displaced. In the absence of any stabilizing ligands, or metal-containing molecules acting as two

* Corresponding author.

SSDI 0022-328X(94)05055-G

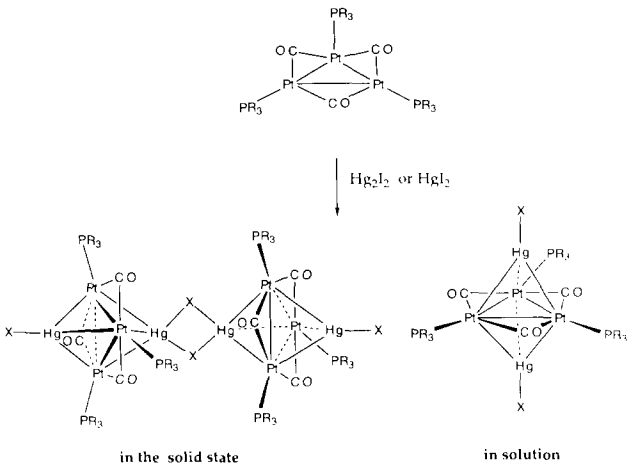

Scheme 1.

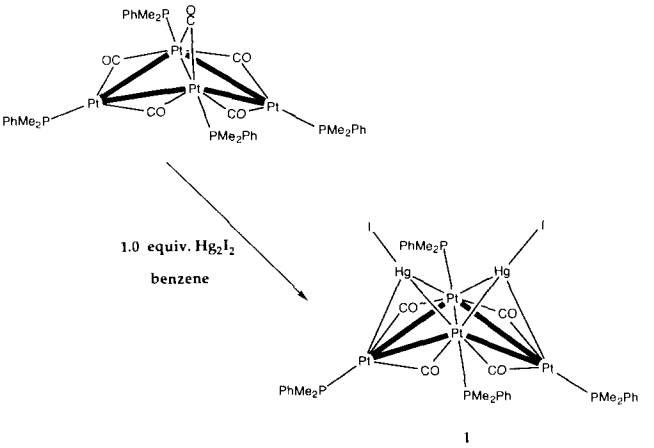

Scheme 2.

electron donors, the 4:5:4 shows a tendency to rearrange to give a 3:3:3 type of cluster, as has been reported for the $[Pt_4(\mu\text{-}CO)_5(PBz_3)_4]$ [5].

Although the Pd-cluster chemistry is different from that of the Pt-cluster [19], the reaction of the $[Pd_4(\mu\text{-}CO)_5(PEt_3)_4]$ with $[C_9H_8NCH(CH_3)HgBr]$ to $[\{Pd_4(\mu\text{-}CO)_4(PEt_3)_4\}\{\mu_3\text{-}HgBr\}_2]$ [21] emphasizes this prediction. Furthermore, very recently, Furmanova et al. have synthesized the related Pt-cluster $[\{Pt_4(\mu\text{-}CO)_4(PPh_3)_4\}\{\mu_3\text{-}HgCF_3\}_2]$ by reacting $[Pt_3(\mu\text{-}CO)_3(PPh_3)_4]$ with $[CF_3HgBr]$ [20].

Therefore, it might be expected that clusters of the type $[Pt_4(\mu\text{-}CO)_5(PR_3)_4]$ can react as building blocks and that in the presence of Hg_2X_2, which can provide two HgX units each of which can act as one electron donor, they could retain the butterfly structure.

This paper reports the reaction of the building block $[Pt_4(\mu\text{-}CO)_5(PMe_2Ph)_4]$ with Hg_2I_2 which gives the Pt_4Hg_2-heterometallic cluster $[\{Pt_4(\mu\text{-}CO)_4(PMe_2Ph)_4\}\{\mu_3\text{-}HgI\}_2]$. [1] The reaction is shown in Scheme 2.

Compound **1** was characterized by X-ray crystal structure determination and by NMR and IR spectroscopy.

2. Results and discussion

The addition of Hg_2I_2 to $[Pt_4(\mu\text{-}CO)_5(PMe_2Ph)_4]$ in benzene gives a green solution, from which orange crystals can be obtained by addition of hexane, in a yield of 55% (see Scheme 2).

The ORTEP view of the cluster core of **1** (Fig. 1) shows that this is indeed the case. It is noteworthy that the reactions of both 3:3:3 and the 4:5:4 cluster with Hg_2X_2 lead formally to an insertion reaction of the cluster into an Hg–Hg bond.

In order to compare the distances of $[\{Pt_4(\mu\text{-}CO)_4(PMe_2Ph)_4\}\{\mu_3\text{-}HgI\}_2]$ (**1**) with those of the basic cluster $[Pt_4(\mu\text{-}CO)_5(PMe_2Ph)_4]$, two different modifications of the latter compound having slightly different structural parameters have to be considered [22]. Se-

Table 1
Types of heterometallic clusters obtained by the reaction of Pt_3-building block {B} with Lewis acids or Lewis bases

Building Block {B}	Lewis Acid/base	Product	Type	Ref.
$[Pt_3(\mu\text{-}CO)_3(PR_3)_3]$	MPR_3^+ [a]	$[\{B\}\{MPR_3\}]^+$	II	[1,5]
$[Pt_3(\mu\text{-}CO)_3(PR_3)_3]$	M^+ [a]	$[\{B\}_2M]^+$	I	[3–5]
$[Pt_3(\mu\text{-}CO)_3(PR_3)_3]$	MX_n [b]	$[\{B\}\{MX_n\}]^+$	II	[5,11]
$[Pt_3(\mu\text{-}CO)_3(PR_3)_4]$	MPR_3^+ [a]	$[\{B\}\{MPR_3\}]^+$	II	[12–14]
$[Pt_3(\mu\text{-}CO)_3(PR_3)_2(dppp)]$	$AgPR_3^+$	$[\{B\}\{AgPR_3\}]^+$	II	[27]
$[Pt_3(\mu\text{-}Cl)(SO_2)_2(PR_3)_3]$	$AuPR_3^+$	$[\{B\}\{AuPR_3\}_2]^+$	III	[7]
$[Pt_3(\mu\text{-}CNXyl)(SO_2)_2(PR_3)_3]$	$AuPR_3^+$	$[\{B\}\{AuPR_3\}]^+$	II	[6]
$[Pt_3(\mu\text{-}CNR)_x(\mu\text{-}CO)_{3-x}(CNR)_y(PR_3)_{3-y}]$ [c]	MPR_3^+ [a]	$[\{B\}\{MPR_3\}]^+$	II	[10]
$[Pt_3(\mu\text{-}CO)_3(PR_3)_3]$	Hg^0	$[\{B\}_2Hg]$, $[\{B\}Hg]$	I, II	[15]
$[Pt_3(\mu_3\text{-}CO)(dppm)_3]^{2+}$	Hg^0	$[\{B\}Hg]^{2+}$	I	[2]
$[Pt_3(\mu_3\text{-}CO)(dppm)_3]^{2+}$	Hg^0	$[\{B\}Hg_2]^{2+}$	III	[2]
$[Pt_3(\mu\text{-}CO)_3(PR_3)_3]$	Tl^I	$[\{B\}Tl]^+$	II	[16]
$[Pt_3(\mu\text{-}CO)_3(PR_3)_3]$	Hg_2X_2	$[\{B\}\{HgX\}_2]$	III	[17]

[a] $M = Cu^I$, Ag^I, Au^I.
[b] $MX_n = ZnX_2$, CdX_2, InX_3.
[c] $x = 2$, $y = 1$ or $x = 3$, $y = 2$, dppp = $Ph_2P(CH_2)_2PPh_2$; dppm = $Ph_2PCH_2PPh_2$.

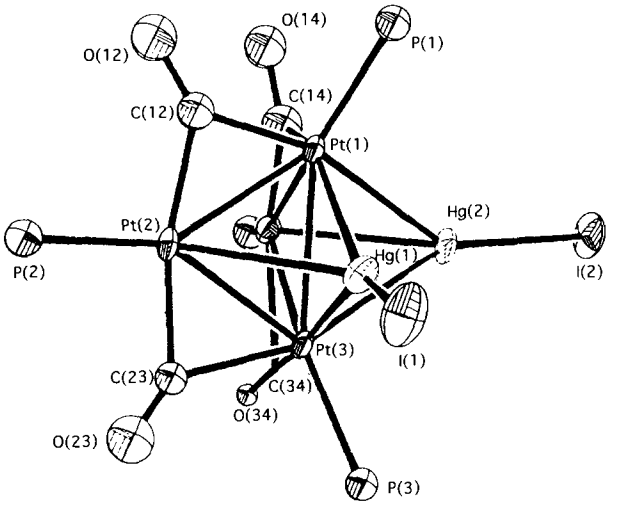

Fig. 1. A view of the structure of $[\{Pt_4(\mu\text{-}CO)_4(PMe_2Ph)_4\}\{\mu_3\text{-}HgI\}_2]$ (1).

lected bond lengths of these compounds are given in Table 2.

Cluster **1** retains the original butterfly structure of 4:5:4, but the central bridging CO molecule has been replaced by an X–Hg–Hg–X fragment. Each of the mercury atoms is bonded to the two bridging platinum atoms and to only one of the external platinum atoms.

Given the skeletal arrangement, the structure of this cluster should have had a mirror plane symmetry. However, this was not found because of differing Pt–Pt and Pt–Hg distances. Whereas Pt(1)–Pt(2) and Pt(1)–Pt(4) distances have the same value of 2.728(3) Å, this is not the case for the Pt(3)–Pt(4) and Pt(3)–Pt(2) distances (2.734(3) and 2.714(3) Å, respectively). For $[Pt_4(\mu\text{-}CO)_5(PMe_2Ph)_4]$ all Pt–Pt distances, except the CO bridged Pt–Pt bond, are in the range of 2.706–2.754 Å [22]. Therefore, the replacement of the bridging CO ligand between Pt(1)–Pt(3) by two Hg-atoms is accompanied by a lengthening of this distance from 2.731(3) Å in $[Pt_4(\mu\text{-}CO)_5(P(Me_2Ph)_3)_4]$ to 3.011(3) Å in $[\{Pt_4(\mu\text{-}CO)_4(PMe_2Ph)_4\}\{\mu_3\text{-}HgI\}_2]$ (**1**). The triangular wings are capped asymmetrically by the Hg atoms as shown by the Hg–Pt distances which differ significantly, varying between 2.716(3) and 3.163(3) Å, the long Hg–Pt distances being those to the platinum wing atoms. Comparable results have been reported for the platinum cluster $[\{Pt_4(\mu\text{-}CO)_4(PPh_3)_4\}\{\mu_3\text{-}HgCF_3\}_2]$ [20] where the Hg–Pt distances range from 2.719(1) to 3.159(1) Å and for the palladium cluster $[\{Pd_4(\mu\text{-}CO)_4(PEt)_3)_4\}\{\mu_3\text{-}Hg_2Br_2\}]$ [21] with Hg–Pd distances from 2.704(1) to 2.993(1) Å. Furthermore, Pt–Hg distances of 2.931(2)–3.084(1) Å were found for $[\{Pt_3(\mu\text{-}CO)_3(PR_3)_3\}\{\mu_3\text{-}Hg\}]_2$.

The Hg–Hg distance of 3.395(4) Å in $[\{Pt_4(\mu\text{-}CO)_4(PMe_2Ph)_4\}\{\mu_3\text{-}HgI\}_2]$ (**1**) is very long and, therefore, there is probably no significant Hg–Hg interaction. Other reported Hg–Hg distances for Hg-contain-

Table 2
Selected Bond Lengths (Å) and Angles (deg) for $[\{Pt_4(\mu\text{-}CO)_4(PMe_2Ph)_4\}\{\mu_3\text{-}HgI\}_2]$ (**1**) (bridging CO's have been omitted for clarity

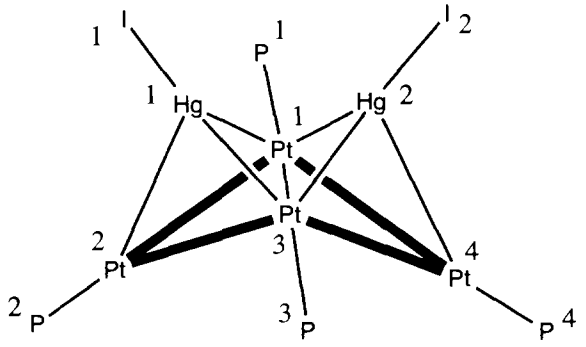

Hg(1)–Pt(1)	2.748(3)	Pt(1)–Pt(2)	2.728(3)
Hg(1)–Pt(2)	3.071(3)	Pt(1)–Pt(3)	3.011(3)
Hg(1)–Pt(3)	2.813(3)	Pt(1)–Pt(4)	2.728(3)
Hg(2)–Pt(1)	2.791(3)	Pt(2)–Pt(3)	2.714(3)
Hg(2)–Pt(3)	2.716(3)	Pt(3)–Pt(4)	2.734(3)
Hg(2)–Pt(4)	3.163(3)	Hg(1)–I(1)	2.704(5)
Hg(1)–Hg(2)	3.395(4)	Hg(2)–I(2)	2.711(5)
Pt(2)–Pt(1)–Pt(4)	75.9(1)	Pt(2)–Pt(1)–Hg(1)	68.2(1)
Pt(3)–Pt(1)–Pt(4)	56.6(1)	Pt(4)–Pt(1)–Hg(1)	114.9(24)
Hg(1)–Pt(1)–Hg(2)	75.6(1)	Pt(3)–Pt(1)–Hg(2)	55.7(1)
Pt(3)–Pt(1)–P(1)	148.6(4)	Hg(1)–Pt(1)–P(1)	99.5(4)
Pt(1)–Pt(2)–Hg(1)	56.2(1)	Pt(1)–Pt(3)–Hg(2)	58.1(1)

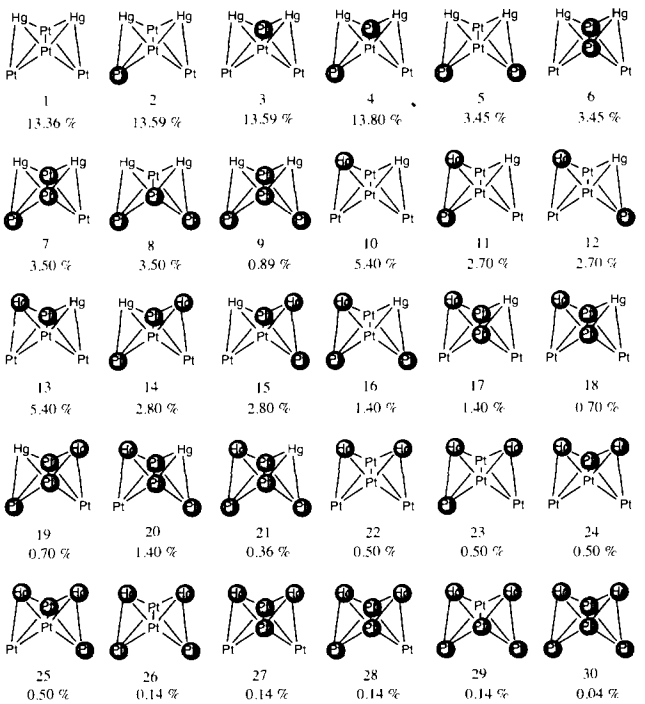

(Pt denotes a magnetically active Pt-nucleus, while ● denotes a ^{195}Pt-atom; same is valid for Hg; ^{31}P-nuclei have not been denoted as their natural abundance is 100%.)

Scheme 3.

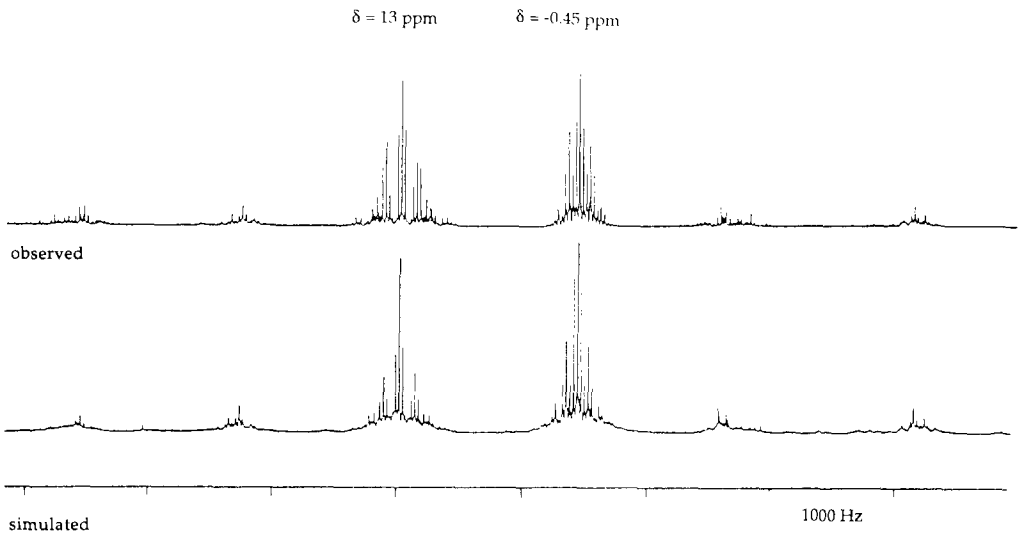

Fig. 2. Observed (upper trace) and calculated (lower trace) $^{31}P\{^1H\}$-NMR spectrum of $[\{Pt_4(\mu\text{-}CO)_4(PMe_2Ph)_4\}\{\mu_3\text{-}HgI\}_2]$ (1).

ing clusters are: $[\{Pt_4(\mu\text{-}CO)_4(PPh_3)_4\}\{\mu_3\text{-}HgCF_3\}_2]$ [20], 3.640 Å; $[\{Pd_4(\mu\text{-}CO)_4(PEt)_3)_4\}\{\mu_3\text{-}Hg_2Br_2\}]$ [21], 3.251(1) Å; $[C(HgCN)_4]$ [23], 3.280–3.398 Å; $[C(HgOAc)_4]$ [24], 3.251–3.436 Å and 3.131–3.149 Å for the heteronuclear cluster $[Rh_4Hg_6(PMe_3)_{12}]$ [25].

The IR pattern of the carbonyl stretching frequencies of **1** are different from those of the $[Pt_4(\mu\text{-}CO)_5(PMe_2Ph)_4]$. Compared to the latter, frequencies are all shifted to higher frequencies and show intense adsorption bands at 1865, 1830, 1802 and 1789 cm^{-1}. This behaviour suggests a weakening of the π-back-bonding from the platinum to the carbonyl ligand which would cause a lengthening of the M–CO bond and a strengthening of the C–O bond. However due to the dynamics of these clusters such bond length changes can not be confirmed by the X-ray structure. In general correlation between the IR shift frequencies and the C–O bond length cannot be easily given [26,10].

While the butterfly cluster $[Pt_4(\mu\text{-}CO)_5(P(Me_2Ph)_3)_4]$ have simple NMR spectra, because all phosphorus and platinum atoms appear chemically identical [22], due to the fast dynamic behaviour in the NMR

Table 3
$^{31}P\{^1H\}$ and ^{195}Pt NMR data for $[\{Pt_4(\mu\text{-}CO)_4(PMe_2Ph)_4\}\{\mu_3\text{-}HgI\}_2]$ (1) (bridging CO's have been omitted for clarity)

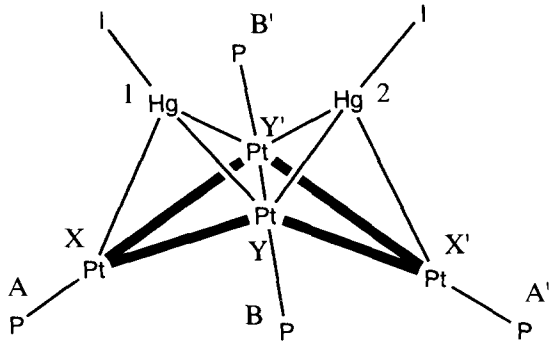

	ppm	Hg^1	Hg^2	Pt^X	$Pt^{X'}$	Pt^Y	$Pt^{Y'}$	P^A	$P^{A'}$	P^B	$P^{B'}$
P^A	−0.5	277	u.	5400	161	173	173	–	7	29	29
$P^{A'}$	−0.5	u.	277	161	5400	173	173	7	–	29	29
P^B	13.0	384	384	253	253	5160	446	29	29	–	43
$P^{B'}$	13.0	384	384	253	253	446	5160	29	29	43	–
Pt^X	−4762	u.	u.	–	u.	1650	1650	5400	161	253	253
$Pt^{X'}$	−4762	u.	u.	u.	–	1650	1650	161	5400	253	253
Pt^Y	−4370	4050	4050	1650	1650	–	1860	173	173	5160	446
$Pt^{Y'}$	−4370	4050	4050	1650	1650	1860	–	173	173	446	5160
Hg^1	u.	–	0	u.	u.	4050	4050	–	–	–	–
Hg^2	u.	0	–	u.	u.	4050	4050	–	–	–	–

u. = unidentifiable

time scale, the ^{31}P- and ^{195}Pt-NMR spectra of **1** are quite complex. It is found that, upon coordination of the two HgI moieties phosphorus and platinum atoms are no longer chemically equivalent and NMR spectroscopy can therefore distinguish bridge atoms and wing atoms. The combinations of the NMR ^{195}Pt atoms (s = 1/2; natural abundance, n.a. = 33.7%), ^{31}P (s = 1/2; n.a. = 100%) and ^{199}Hg atoms (s = 1/2; n.a. = 16.8%) leads to the formation of 64 isotopomers. After subtraction of equal and enantiomeric structures, one is left with 30 isotopomers (sketched in Scheme 3) which are responsible for the NMR spectra.

The spectroscopic simplest isotopomer (1), i.e., that without NMR active platinum and mercury atoms gives rise to an A_2M_2 spin system, the difference in chemical shifts of the two types of phosphorus being sufficiently large to avoid the formation of an A_2B_2 spin system. Therefore, the ^{31}P-NMR spectrum (see Fig. 2) shows two triplets one centred at 13 ppm (^{31}P on the bridge atoms) and the other at −0.45 ppm (^{31}P on the wing atoms). The presence of one ^{195}Pt results in the formation of two isotopomers one with ^{195}Pt on the wing atom isotopomer (2) or on the bridge atom isotopomer (3). As the resonances are well separated and the two different $^1J(Pt-P)$ constants are in the range of 5160 Hz, the ^{31}P-NMR spectrum of this species can be analyzed by a (pseudo) first order approach. Therefore, the actual spin systems, $AA'M_2X$ and $A_2MM'Y$, respectively, can be treated as M_2PQX and MNP_2Y, respectively where P, Q and N, M are isochronous. The X and Y part of these isotopomers, 2 and 3, cause the formation of two doublets of triplets, which are doubled again. This pattern allows the calculation of the

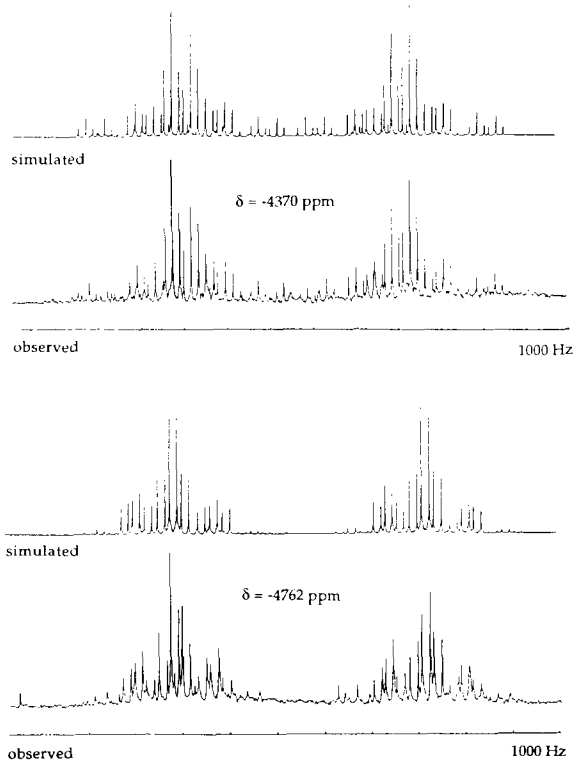

Fig. 3. Observed (upper trace) and calculated (lower trace) ^{195}Pt-NMR spectrum of $[\{Pt_4(\mu\text{-}CO)_4(PMe_2Ph)_4\}\{\mu_3\text{-}HgI\}_2]$ (**1**).

Table 4
Structural determination summary for $[\{Pt_4(\mu\text{-}CO)_4(PMe_2Ph)_4\}\{\mu_3\text{-}HgI\}_2]$(1)

Crystal data	
Empirical formula	C36H44Hg2I2O4P4Pt4
Colour; habit	red; cube
Crystal size (mm^3)	0.2×0.2×0.2
Crystal system	Monoclinic
Space group	$P21/n$
Unit cell dimensions	a = 10.086(2), b = 18.739(4), c = 24.764(5) Å, β = 90.94(3)°
Volume	4679.8(17) Å^3
Z	4
Formula weight	2099.9 g
Density(calc.)	2.980 g m^{-3}
Absorption coefficient	19.939 mm^{-1}
F(000)	3720
Data collection / diffractometer used	
Siemens	R3m
Radiation	Mo Kα (λ = 0.71073 Å)
Temperature (K)	298
Monochromator	Highly oriented graphite crystal
2θ Range	3.0 to 40.0°
Scan type	2θ-ω
Scan speed	Variable; 2.00 to 10.00° min^{-1} in ω
Scan range (ω)	1.20° plus Kα separation
Background measurement	Stationary crystal and stationary counter at beginning and end of scan, each for 25.0% of total scan time
Standard reflections	1 measured every 100 reflections
Index ranges	$-9 \le h \le 9$, $0 \le k \le 18$, $0 \le h \le 23$
Reflections collected	4373
Independent reflections	4373(R_{int} = 0.00%)
Observed reflections	3303 ($F \ge 3.0\ \sigma(F)$)
Absorption correction	n/a
Solution and Refinement	
System used	Siemens SHELXTL PLUS (VMS)
Solution	Direct Methods
Refinement method	Full-Matrix Least-Squares
Quantity minimized	$\Sigma w(F_o - F_c)^2$
Absolute structure	n/a
Extinction correction	n/a
Hydrogen atoms	Riding model, fixed isotropic U
Weighting scheme	$w^{-1} = \Sigma \wedge 20(F) + 0.0000F \wedge 20$H
Number of parameters refined	267
Final R indices (obs. data)	R = 7.87%, wR = 7.64%
R indices (all data)	R = 9.97%, wR = 7.68%
Goodness-of-fit	4.40
Largest and mean Δ/σ	0.334, 0.009
Data-to-parameter ratio	12.4:1
Largest difference peak	3.67 eÅ^{-3}
Largest difference hole	−3.39 eÅ^{-3}

coupling constants $^{1}J(Pt^{X}, P^{A})$, $^{2}J(Pt^{X}, P^{A'})$ and $^{2}J(Pt^{X}, P^{M})$.

The introduction of a further ^{195}Pt-isotope leads to the formation of three new isotopomers. Only isotopomer 4, with n.a. = 13.8%, makes a significant contribution to the NMR spectrum. This pattern may be simply explained by a further splitting of the resonances of isotopomer (2) by the additional NMR-active atom.

The main pattern of the ^{195}Pt-NMR spectrum which arises mainly from isotopomers (2) and (3) leading to two doublets of triplets are doubled again. The chemical shifts are for the bridging atoms and for the wing atoms are −4370 and −4762 ppm, respectively. While in the ^{31}P spectrum ^{199}Hg satellites cannot be detected due to the low natural abundance of the isotopomers, only the resonances of the bridge atoms to ^{199}Hg are detectable in the ^{195}Pt spectrum (see Fig. 3). This may be explained by the fact that the μ_3-Hg moieties is attached to two bridging platinum atoms (isotopomer 13; n.a. 5.4%), but only one of the wing platinum atoms (isotopomer 11; n.a. 2.7%). The NMR spectra of **1** can be simulated for both ^{31}P- and ^{195}Pt-NMR satisfactorily and the values obtained are given in Table 3.

The compound reported by Furmanova et al. [20], $[\{Pt_4(\mu\text{-}CO)_4(PPh_3)_4\}\{\mu_3\text{-}HgCF_3\}_2]$, is related to **1** and is particularly interesting in this context. This reaction shows that a 3:3:4 cluster undergoes a rearrangement. Similar rearrangements have been extensively studied in this laboratory [26].

In order to use a cluster of 3:3:4 type as a building block, without loss of the basic unit structure, one should abstract a halide from the RHgX. The resulting $R\text{–}Hg^{+}$ fragment is isolobal to the $AuPR_3^{+}$ or $CuPR_3^{+}$ fragment and might therefore react with a 3:3:4 unit as was shown by the formation of $[\{3:3:4\}\{CuPR_3\}]^{+}$ [12]. However, preliminary experiments in our laboratory showed that, in presence of light, the 3:3:3 clusters react rapidly with compounds such as PhHgX, BzHgX by a radical mechanism with organo–mercury bond disruption and formation of clusters of the type $[\{333\}\{\mu_3\text{-}HgX\}_2]$ [17].

3. Experimental section

The chemical operations routinely used standard Schlenk line procedures under an atmosphere of pure argon and dry O_2-free solvents.

The infrared spectrum was recorded on a Perkin-Elmer 1420 spectrometer as an RbI pellet. The ^{31}P–$\{^{1}H\}$ and ^{195}Pt–$\{^{1}H\}$ spectra were run on a Bruker WM250 spectrometer. The ^{31}P and ^{195}Pt operating frequencies were 101.3 and 53.5 MHz, respectively, and reported relative to H_3PO_4 (85%) and Na_2PtCl_6, respectively as an internal standard. ^{31}P-$\{^{1}H\}$-NMR and ^{195}Pt-$\{^{1}H\}$ simulations were carried out using the program PANIC developed by Bruker.

Table 5
Atom coordinates ($\times 10^4$) and equivalent isotropic displacement coefficients ($Å^2 \times 10^3$)

Atom	x	y	z	U_{eq}*
Pt(1)	2267(2)	1429(1)	1309(1)	26(1)
Pt(2)	1999(2)	2877(1)	1281(1)	28(1)
Pt(3)	−106(2)	2185(1)	828(1)	24(1)
Pt(4)	1(2)	1682(1)	1864(1)	28(1)
C(12)	3927(70)	2165(41)	1094(36)	120(17)
C(23)	−65(71)	3175(43)	1158(36)	120(17)
C(34)	−1691(73)	2064(52)	1476(30)	120(17)
C(14)	1831(72)	1258(49)	2047(31)	120(17)
O(14)	2305(45)	986(25)	2455(19)	69(15)
O(23)	−411(47)	3765(27)	933(19)	79(16)
O(34)	−2634(47)	2432(26)	1559(19)	77(16)
O(12)	4670(59)	2332(33)	1746(25)	129(23)
Hg(1)	2257(2)	1942(1)	269(1)	35(1)
Hg(2)	126(3)	742(1)	805(1)	37(1)
I(1)	3758(5)	2140(3)	−613(2)	57(2)
I(2)	−1231(5)	−491(2)	647(2)	57(2)
P(1)	3832(16)	568(10)	1235(6)	38(6)
P(2)	2906(18)	3967(9)	1335(8)	45(7)
P(3)	−1637(16)	2299(8)	128(7)	39(6)
P(4)	−1061(16)	1440(9)	2632(7)	39(7)
C(101)	3533(79)	−316(43)	1525(31)	82(26)
C(102)	4524(82)	−692(43)	1706(30)	85(26)
C(103)	4089(83)	−1360(45)	1991(31)	98(29)
C(104)	2862(59)	−1577(33)	2046(22)	41(17)
C(105)	1725(82)	−1259(42)	1872(29)	89(27)
C(106)	2099(57)	−502(31)	1655(22)	37(17)
C(107)	5561(62)	815(39)	1449(27)	81(25)
C(108)	4260(72)	226(42)	579(27)	96(29)
C(201)	3035(58)	4389(33)	644(24)	41(17)
C(202)	2234(61)	4976(34)	520(25)	52(20)
C(203)	2455(67)	5151(38)	−26(28)	65(22)
C(204)	3252(68)	4823(39)	−368(30)	68(23)
C(205)	3881(71)	4311(41)	−198(30)	76(24)
C(206)	3819(54)	4034(30)	308(22)	32(16)
C(207)	4944(80)	3973(50)	1440(36)	148(42)
C(208)	1839(53)	4652(29)	1777(22)	38(17)
C(301)	−1153(48)	2796(27)	−432(20)	20(14)
C(302)	−1951(63)	2813(35)	−892(25)	57(20)
C(303)	−1263(68)	3185(37)	−1427(28)	68(23)
C(304)	−262(63)	3576(36)	−1392(27)	54(20)
C(305)	546(82)	3599(45)	−972(32)	97(29)
C(306)	42(55)	3246(30)	−476(23)	39(17)
C(307)	−2091(67)	1489(36)	−267(28)	80(25)
C(308)	−3079(48)	2736(28)	335(21)	33(16)
C(401)	−1777(53)	565(30)	2640(23)	33(16)
C(402)	−1541(59)	78(33)	2224(25)	47(18)
C(403)	−2008(64)	−647(39)	2301(30)	67(22)
C(404)	−2632(60)	−872(35)	2713(25)	49(19)
C(405)	−2905(58)	−313(33)	3139(25)	47(19)
C(406)	−2379(50)	354(29)	3104(21)	27(15)
C(407)	−56(55)	1504(32)	3269(22)	47(19)
C(408)	−2507(52)	2060(30)	2793(22)	42(17)

U_{eq}* Equivalent isotropic U defined as one third of the trace of the orthogonalized U_{ij} tensor

3.1. Synthesis of $[\{Pt_4(\mu\text{-}CO)_4(PMe_2Ph)_4\}\{\mu_3\text{-}HgI\}_2]$ (1)

$[Pt_4(\mu\text{-}CO)_5(P(Me_2Ph)_3)_4]$ 100 mg, (0.068 mmol) was dissolved under argon in benzene (10 ml) and Hg_2I_2 (44 mg, 0.069 mmol) was added. The colour changed from red to green after a few minutes. After addition of hexane a orange yellow solution was obtained from which, after a few days at 8°C, crystals could be obtained. Yield: 55%, 78 mg.

3.2. Crystal structure determination of compound 1

A red cube was placed on a Picker-Stoe-Diff-4 diffractometer which was used for the determination of lattice parameters, space group, and data collection. The cell parameters were obtained by a least-squares fit of the 2θ values of 16 high-angle reflections ($17.4° \leq 2\theta \leq 20.8°$). The crystallographic data are listed in Table 4.

A total of 4373 reflections was measured in the 2θ range of 3–40°. During data collection one standard reflection (2, −1, 10) was measured every 120 minutes. No significant variations of the intensities were observed. At 2θ values higher than 40° the intensities of the reflections were very low because of the poor quality of the crystal, therefore the measurement was stopped at this angle. Data were corrected for Lorentz and polarization factors, and no empirical or numerical absorption correction was applied. Reflections having $I \geq 4\sigma(I)$ were considered as observed and thus 3151 reflections were used for the solution and refinement of the structure.

The structure was solved by direct and Fourier methods using the SHELXTL-Plus system. Refinement was carried out by full-matrix least-squares; the function minimized was $\Sigma w(|F_o| - 1/k|F_c|)^2$. The positions of the hydrogen atoms were calculated but not refined. Anisotropic temperature factors were used for the Pt, Hg, P and I atoms, all other atoms were refined isotropically. Scattering factors were taken from International Tables of X-ray Crystallography, Kynoch; Birmingham, 1974. The thermal displacement parameters of all four carbonyl groups were refined as a single parameter for the carbon and the oxygen atom. The final positions of the atoms are listed in Table 5.

Acknowledgement

We gratefully acknowledge the support of the Schweizerischer Schulrat.

Supplementary Material Available

The structure determination summary, data collection, solution and refinement, tables of atomic coordinates and equivalent isotropic displacement coefficients, H-atom coordinates and isotropic displacement coefficients (2 pages); tables of observed and calculated structure factors (10 pages) have been deposited at the Cambridge Crystallographic Data Centre. Enquiries for copies of these materials can also be directed to the corresponding authors.

References

[1] C.E. Briant, R.W.M. Wardle and D.M.P. Mingos, *J. Organomet. Chem., 267* (1984) C49.
[2] G. Schoettel, J.J. Vittal and R.J. Puddephatt, *J. Am. Chem. Soc., 112* (1990) 6400.
[3] A. Albinati, K.-H. Dahmen, A. Togni and L.M. Venanzi, *Angew. Chem. Int. Ed. Engl., 24* (1985) 766.
[4] M.F. Hallam, D.M.P. Mingos, T. Adatia and M. McPartlin, *J. Chem. Soc., Dalton Trans.*, (1988) 335.
[5] K.-H. Dahmen, Ph.D. Thesis, ETH Zürich, 8177, 1986.
[6] C.M. Hill, D.M.P. Mingos, H. Powell and M.J. Watson, *J. Organomet. Chem., 441* (1992) 499.
[7] D.M.P. Mingos, P. Oster and D.J. Sherman, *J. Organomet. Chem., 320* (1987) 257.
[8] D.M.P. Mingos and R.W.M. Wardle, *J. Chem. Soc., Dalton Trans.*, (1986) 73.
[9] N.C. Payne, R. Ramachandran, G. Schoettel, J.J. Vittal and R.J. Puddephatt, *Inorg. Chem., 30* (1991) 4048.
[10] D. Imhof, U. Burckhardt, K.-H. Dahmen and H. Rüegger, *Inorg. Chem., 32* (1993) 5206.
[11] A. Stockhammer, K.-H. Dahmen, T. Gerfin, L.M. Venanzi, V. Gramlich, and W. Petter, *Helv. Chim. Acta., 74* (1991) 989.
[12] P. Braunstein, S. Freyburger and O. Bars, *J. Organomet. Chem., 352* (1988) C29.
[13] J.J. Bour, R.P.F. Kanters, P.P.J. Schlebos, W. Bos, W.P. Bosman, H. Behm, P.T. Beurskens and J.J. Steggerda, *J. Organomet. Chem., 329* (1987) 405.
[14] S. Bhaduri, K. Sharma, P.G. Jones and C.F. Erdbrugger, *J. Organomet. Chem., 326* (1987) C46.
[15] A. Albinati, A. Moor, P.S. Pregosin and L.M. Venanzi, *J. Am. Chem. Soc., 104* (1982) 7672.
[16] O.J. Ezomo, D.M.P. Mingos, I.D. Williams, *J. Chem. Soc., Chem. Commun.*, (1987) 924.
[17] A. Albinati, K.-H. Dahmen, F. Demartin, J.F. Forward, C.J. Longley, D.M.P. Mingos and L.M. Venanzi, *Inorg. Chem., 31* (1992) 2223.
[18] L.H. Gade, *Angew. Chem. Int. Ed. Engl.*, 32 (1993), 24.
[19] E.M. Leber, Ph.D. Thesis, ETH Zürich, 9282 1990.
[20] N.G. Furmanova, V.V. Bashilov, S.S. Kurasov, N.K. Eremenko and V.I. Sokolov, *Sov. Phys. Crystallogr., 37* (1992) 325.
[21] E.G. Mednikov, V.V. Bashilov, V.I. Sokolov, L. Slovokhotov and T. Struchkov, *Polyhedron, 2* (1983) 141.
[22] A. Moor, P.S. Pregosin, L.M. Venanzi and A.J. Welch, *Inorg. Chim. Acta., 85* (1984) 103.
[23] D. Grdenic, M. Sikirica and B. Korpar-Colig, *J. Organomet. Chem., 153* (1978) 1.
[24] D. Grdenic and M. Sikirica, *Z. Kristallografic, 150* (1979) 107.
[25] R.A. Jones, F.M. Real, G. Wilkinson, A.M.R. Galas and M.B. Hursthouse, *J. Chem. Soc., Dalton Trans.*, (1981) 126.
[26] K.-H. Dahmen, D. Imhof and L.M. Venanzi, unpublished results.
[27] A.D. Burrow, J.G. Jeffrey, J.C. Machell and D.M.P. Mingos, *J. Organomet. Chem., 406* (1991) 399.